Conversion of Methane to Methanol on Diiron and Dicopper Enzyme Models of Methane Monooxygenase: A Theoretical Study on a Concerted Reaction Pathway

Kazunari Yoshizawa,* Akiya Suzuki, Yoshihito Shiota, and Tokio Yamabe

Department of Molecular Engineering, Kyoto University, Sakyo-ku, Kyoto 606-8501

Institute for Fundamental Chemistry, 34-4 Takano-Nishihiraki-cho, Sakyo-ku, Kyoto 606-8103

(Received September 16, 1999)

We present theoretical analyses for the conversion of methane to methanol on a diiron model of soluble methane monooxygenase (sMMO) and on dicopper models of particulate methane monooxygenase (pMMO) using the hybrid density-functional-theory B3LYP method. Methane is proposed to be reasonably converted into methanol in a two-step concerted manner on the dinuclear enzyme models. The first step in our proposal is concerted H atom abstraction of methane via a four-centered transition state (TS1) and the second step is concerted methyl migration via a three-centered transition state (TS2). The general features of the electronic process are identical to those of the gas-phase process for the methane–methanol conversion by the bare FeO^+ complex. The concerted H atom abstraction and the direct H atom abstraction via a transition state with a linear C–H–O(Fe) array are compared using the dinuclear models. The transition state for the direct H atom abstraction (TSd) on the diiron model is found in the spin undecet state; however, that on the dicopper models is found in the doublet state. Kinetic isotope effects (k_H/k_D) are calculated and analyzed for the concerted and the direct H atom abstraction mechanisms using the transition state theory. Calculated k_H/k_D values for the concerted process and the direct process are 9 and 14, respectively, at 300 K.

Methanotrophic bacteria oxidize methane using molecular dioxygen, leading to methanol, formaldehyde, formic acid, and finally carbon dioxide. In the initial stages of the methane oxidation pathway, this inert hydrocarbon is efficiently converted into methanol by methane monooxygenase (MMO) under physiological conditions.[1] The initial step of methane oxidation has been investigated in two species of methanotrophs: *Methylococcus capsulatus* (Bath) and *Methylosinus trichosporium* OB3b. In both species of methanotrophs, two different forms are known to exist under different conditions: a cytoplasmic (soluble) MMO and a membrane-bound (particulate) MMO. Only soluble MMO (sMMO) has been purified and characterized. X-ray structural analyses[2] have demonstrated that the hydroxylase component of sMMO contains two dinuclear iron clusters in which methane is efficiently converted into methanol. The key intermediate **Q** of sMMO, the species responsible for the direct reactivity toward methane, has been proposed to involve a high-valent dinuclear Fe(IV) complex, in which the two iron active centers are antiferromagnetically coupled.[3] Mechanistic studies have been performed by stopped-flow optical spectroscopy to examine the activated dioxygen intermediates and their reactions with hydrocarbon substrates.[4] It has been suggested from Mössbauer and EXAFS analyses that the active site of intermediate **Q** should involve an $Fe_2(\mu\text{-}O)_2$ "diamond" core,[5] as indicated in Chart 1. Although X-ray structural analysis has not yet been successful for intermediate **Q**, the first coordination sphere around each iron center has been proposed from EXAFS analyses to consist of 4.5 O/N on the average. Several possible mechanisms for the interesting catalytic function of sMMO have been discussed from experimental and theoretical viewpoints.[6] Particulate MMO (pMMO) is a copper-containing membrane protein,[7] but in contrast to sMMO, the structure of the pMMO active site is unknown at present because of difficulty in handling the purified pMMO. In both *Methylococcus capsulatus* (Bath) and *Methylosinus trichosporium* OB3b, methane oxidation is carried out mostly by sMMO under conditions of copper limitation; however, addition of copper to the growth medium significantly increases the activity of pMMO. Thus, although the role of copper in pMMO activity is still not fully understood, copper may play an important role in the methane oxidation by pMMO. Proposals for the structure of the pMMO active site include trinuclear copper(II),[7a] mononuclear copper(II),[8,9] and dinuclear mixed-valent Cu(II)Cu(III) clusters.[10] Recently, the di-μ-oxo dicopper diamond core, indicated in Chart 1, has been proposed from model studies to be responsible for dioxygen activation and hydrocarbon oxidation.[11—13] Similar results have been observed in other dinuclear complexes of di-μ-oxo diamond core.[14]

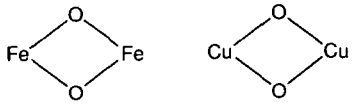

Chart 1.

Determining the mechanism of hydrocarbon hydroxylation in biological systems as well as in man-made catalytic systems is of current interest. The hydroxylation by cytochrome P450 has been considered to occur by a mechanism involving hydrogen atom abstraction from substrate in the initial stages, followed by rapid transfer of the metal-bound hydroxyl radical to the intermediate alkyl radical.[15] This widely-believed radical mechanism is called "oxygen rebound mechanism". The current theoretical proposals can be essentially partitioned into radical[6c,16] and concerted[6d,17] mechanisms. Radical mechanisms[18] have been strongly supported by observed kinetic isotope effects and loss of stereochemistry in substrate carbon. However, recent radical-clock measurements,[19] regioselective hydroxylations,[20] and high degrees of retention of stereochemistry[21] stimulate reinterpretation of the oxygen rebound mechanism.

We have proposed a concerted reaction pathway[22] for the methane–methanol conversion by the bare FeO^+ complex, which occurs under ion cyclotron resonance conditions.[23] Our proposed reaction pathway is indicated in Scheme 1: (1) In the initial stages of the reaction, C_{3v}- or D_{2d}-distorted methane is activated on a coordinatively unsaturated iron-oxo complex to make the methane complex; (2) abstraction of an H atom of methane occurs in a concerted manner via the four-centered transition state (TS1) leading to the reaction intermediate that involves resultant OH and CH_3 ligands; (3) concerted methyl migration via the three-centered transition state (TS2) leads to the methanol complex; (4) each electronic process via TS1 or TS2 is finished in a timescale of 100 fs.[24]

We also proposed that this mechanism is applicable to the methane hydroxylation on intermediate **Q** of sMMO.[17] Moreover, we successfully analyzed the reaction pathway for the direct conversion of benzene to phenol by applying this concerted mechanism.[25] In this article, we extend and refine our two-step concerted mechanism using a diiron model of sMMO and dicopper models of pMMO, demonstrating that the conversion of methane to methanol proceeds in essentially identical ways on the dinuclear enzyme models.

Diiron and Dicopper Models. Our theoretical model of intermediate **Q** of sMMO is indicated in **1** (Chart 2). This model contains an $Fe^{IV}_2(\mu\text{-O})_2$ diamond core with a μ-carboxylato bridge following the suggestion by Münck, Lipscomb, Que, and their collaborators.[5] From EXAFS analyses, the first coordination sphere around the two iron sites of intermediate **Q** has been proposed to consist of 4.5 O/N on the average, as mentioned earlier. It is in general difficult to detect and characterize the real active center of catalysts and enzymes, and this is the sole proposal on the coordination environment of intermediate **Q**. We adopt this proposal. Thus, we set up a diiron model (**1**) in which the two irons are five- and four-coordinate. We used hydroxo ligands to form the four- and five-coordination environments of the iron centers in this model. The formal charge of each iron is +4, that of the oxo species −2, that of the carboxylato bridge −1, and that of the hydroxo ligands −1; as a consequence, the total charge of this model complex is neutral. Although we used a diiron model with +3 charge in a previous study,[17c] we used here a diiron model whose total charge is neutral. This improvement of model will increase the reliability of our computations on the two-step concerted mechanism, but the essential features of the calculational results are identical. This model is relatively small, but it enables us to carry out systematic vibrational analyses, which will greatly increase the quality of our discussions on computed structures and energetics for the reaction pathways. Moreover, we are able to calculate kinetic isotope effects from systematic vibrational analyses. The reason that we use this small model lies in these advantages for theoretical considerations.

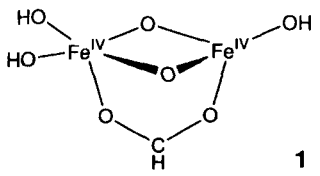

1

Chart 2.

It is difficult to set up a copper-containing complex modeling the active site of pMMO because its structure is currently unknown. As mentioned earlier, a few possibilities have been proposed for the active site of pMMO,[7–10] but no definite conclusion has yet been drawn on the copper–ion arrangement. We tentatively assumed that the active site of pMMO should contain a mixed-valent dinuclear $Cu^{II}Cu^{III}(\mu\text{-O})_2$ diamond core, following the recent suggestion by Chan et al.[10] This assumption may be supported from recent studies on dicopper complexes that successfully catalyze the oxidation of hydrocarbons.[12,13] It is also difficult to set up the coordination

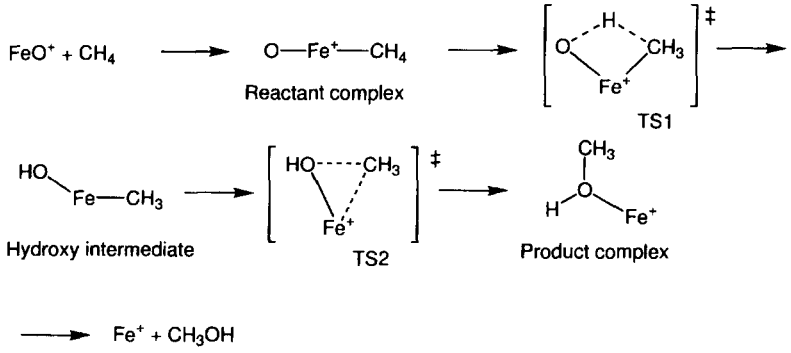

Scheme 1.

environment of the dicopper core. In the context of our concerted mechanism in which binding of methane occurs in the initial stages of the reaction, we assumed model complexes (**2** and **3**) which involve coordinatively unsaturated four-coordinate copper ions and four- and three-coordinate copper ions, respectively. From the viewpoint of known catalytic chemistry, it is in general reasonable to assume that catalytically active metal complexes might be coordinatively unsaturated. To keep the neutrality of the model complexes, we used ammonia and hydroxo ligands, as indicated in Chart 3. The formal charge of the left-hand side copper ion is considered from electron counting to be +2 and that of the right-hand side copper ion is +3.

Method of Calculation. The Gaussian 98 program package[26] was used for hybrid density-functional-theory (DFT)/Hartree–Fock B3LYP calculations.[27,28] Recently this hybrid DFT method has been successfully applied to many catalytic and enzymatic reactions because this method provides excellent descriptions of chemical reaction profiles, particularly in geometries, heats of reaction, and barrier heights. We used the double-ζ valence basis set (8s5p5d)/[3s3p2d][29] with the ECP (effective core potential) replacing core electrons up to 2p for the Fe and Cu atoms and the standard double-ζ basis sets[30] for the H, C, N, and O atoms. These basis sets are referred to as LanL2DZ according to the basis set code of the Gaussian program.

The spin state of the diiron model (**1**) was set to be a singlet, following the Mössbauer observation, and those of the dicopper models **2** and **3** was set to be a doublet. Accordingly, we used the spin-restricted version of the B3LYP method for the reaction species associated with model **1** and the spin-unrestricted version for the reaction species associated with models **2** and **3** in order to obtain a first insight concerning the reaction pathways. We optimized local minima corresponding to reaction intermediates and saddle points corresponding to transition states (TSs) on potential energy surfaces. Vibrational analyses were systematically carried out in order to confirm that all optimized structures correspond to a local minimum that has no imaginary mode of vibration or a saddle point that has only one imaginary mode of vibration. Zero-point vibrational energy corrections were taken into account in calculating the total energies of the reaction intermediates and the transition states.

Clearly, the spin restriction in the framework of the DFT method is not sufficient for the singlet state of the diiron model (**1**) from a theoretical viewpoint, because antiferromagnetic coupling between the two iron ions cannot adequately be described within the spin-restricted version of the DFT method. In fact, it is reasonable to consider that the two Fe(IV) ions are coupled antiferromagnetically in the active site of intermediate **Q** of sMMO. Spin-unrestricted calculations on the singlet potential energy surface may improve the quality of the calculations. However, the principal disadvantage of the spin-unrestricted method is that a resulting wavefunction is no longer spin pure, and thus such a calculation in a singlet state might lead to a wavefunction that is a mixture of a singlet and triplet rather than a pure singlet. When a wavefunction is a mixture of different spin multiplicities, the energy obtained is not reliable at all. The extent of such "spin contamination" can be assessed by examining the expectation value of the S^2 operator, $\langle S^2 \rangle$. Thus, we carefully examined computed $\langle S^2 \rangle$ values when we use the spin-unrestricted method.

Methane–Methanol Conversion on a Diiron Model. We first present in Fig. 1 ball-and-stick structures for the reaction intermediates and the transition states that model the reaction pathway for the methane hydroxylation by sMMO. First coordination distances are indicated in units of Å. In the diamond core of model **1**, the Fe···Fe distance was computed to be 2.656 Å; this value is qualitatively consistent with 2.46 Å, a value estimated from EXAFS analyses for the actual intermediate **Q**.[5] This short Fe···Fe distance is quite reasonable in the singlet state because upper d-block orbitals that are out-of-phase with respect to the Fe–O bonds in the diamond core are not filled, as seen later in this paper. The O···O distance was predicted to be 2.422 Å. Intermediate **Q** is a subject of debate concerning the structure of the active site, so detailed X-ray structural analyses are crucial for a better understanding of the methane hydroxylation by sMMO.

Let us next turn our attention to the conversion of methane to methanol. In the initial stages of the reaction, methane is bound to the four-coordinate iron of model **1**, leading to a reactant (methane) complex. The binding energy was computed to be 6.1 kcal mol^{-1}; thus, methane is successfully bound to this neutral complex, the Fe–C(H_4) distance being 2.831 Å. The driving force for the methane binding is not a charge effect, but orbital interactions, particularly between the t_2 HOMO of methane and unfilled d-block orbitals of the complex, as discussed in our previous papers.[17b,17c] In such methane complexes, C_{3v}- or D_{2d}-type deformation of methane is expected to take place from ab initio computations at various theoretical levels.[31] In this case, the methane molecule is deformed into a C_{3v}-type structure.

Methane complexes have been repeatedly proposed to be involved in the C–H bond activation of methane; extensive indirect data have been obtained to support the intermediary of methane complexes.[32] A clear example of methane complex was recently obtained by Billups et al.[32i] The neutral Co(CH_4) complex was formed during photolysis of the CH_3CoH complex in an argon matrix; the threefold degenerate T_2 vibrational mode of methane at 1305.3 cm^{-1} was observed from FTIR measurements to split into two peaks at

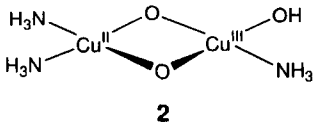

2

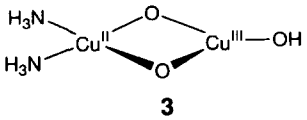

3

Chart 3.

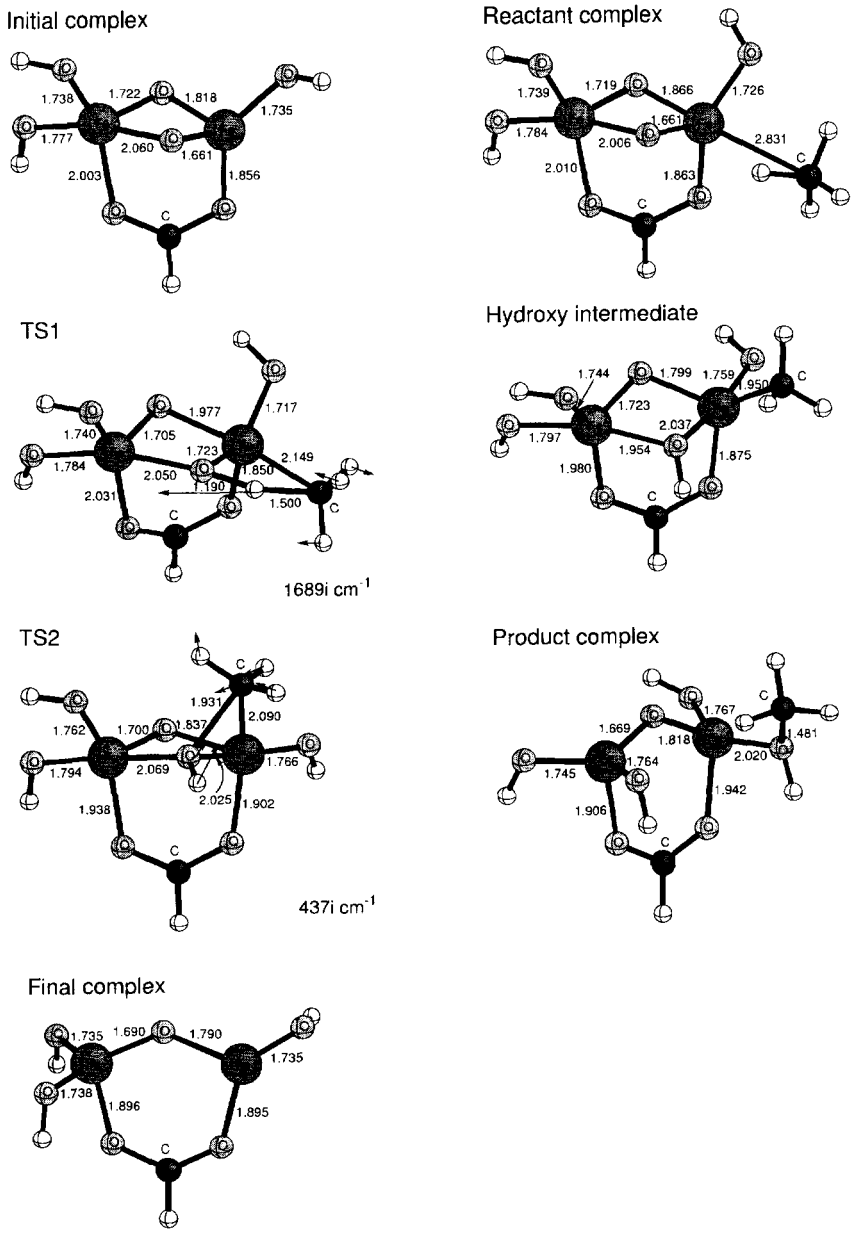

Fig. 1. Computed structures for the reaction intermediates and the transition states (TS1 and TS2) for the conversion of methane to methanol by a diiron model complex of sMMO (**1**). Bond distances in Å. Imaginary modes of vibration that characterize the transition states are indicated.

1303.4 and 1299.3 cm^{-1} in the $Co(CH_4)$ complex, implying that the methane complex is a C_{3v} species. It is thus useful to look at the vibrational analysis of the methane complex. Computed values of the molecular vibrations of free methane and the methane bound to model **1** are listed in Table 1. Agreement with experiment is excellent for the vibrational frequencies, calculated wavenumbers of free methane being accurate within a range of 3—6%. Since the methane in the diiron complex is deformed into a nearly C_{3v} structure, the T_2 modes of C–H stretching and C–H bending are split into two components.

After the formation of the methane complex, concerted H atom abstraction takes place at one of the iron centers via the four-centered transition state (TS1) to lead to the hydroxy intermediate, as shown in Fig. 1. The general features of this C–H cleavage pathway are identical to those of the gas-phase reaction in the FeO^+/CH_4 system.[22] This transition state is well characterized by a single imaginary mode of vibration (1689i cm^{-1}), this high frequency implying that this transition state is responsible for C–H bond dissociation. The dissociating C–H distance of 1.500 Å and the forming O–H distance of 1.190 Å are quite appropriate for this concerted electronic process. The activation barrier for TS1 was computed to be 37.5 kcal mol^{-1} on the singlet potential energy surface when measured from the reactant complex and 31.4 kcal mol^{-1} from the dissociation limit. These values are large compared to the values in the gas-phase reaction (31.1 kcal mol^{-1} on the sextet state and 15.7 kcal mol^{-1} in

Table 1. Computed Vibrational Frequencies (in cm^{-1}) of Free Methane and the **1**(CH_4) Complex at the B3LYP/LanL2DZ Level of Theory
Observed vibrational frequencies of free methane are also listed.

CH_4	**1**(CH_4) singlet	**1**(CH_4) triplet	CH_4 (obs)
3170 (T_2)	3185	3197	3019 (T_2)
	3167	3157	
	3118	3117	
3030 (A_1)	3005	3005	2917 (A_1)
1582 (E)	1606	1601	1534 (E)
	1580	1578	
1386 (T_2)	1405	1412	1306 (T_2)
	1387	1383	
	1384	1367	

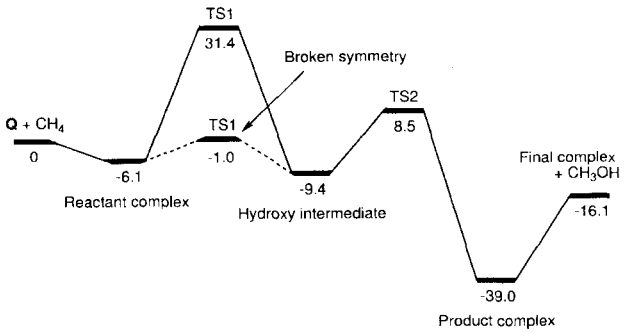

Fig. 2. Energetics for the conversion of methane to methanol by a diiron model complex of sMMO (**1**) on the singlet potential energy surface. Energies in kcal mol^{-1}.

the quartet state). We think that this shortcoming comes from our calculations performed within the framework of the spin-restricted version of the B3LYP/LanL2DZ method. Since the spin-unrestricted version of this method may improve the energetics, we carried out calculations in the singlet state of the diiron complex. We successfully obtained a symmetry-broken solution for TS1, the computed spin density on one iron ion being +2.14 and that on the other iron ion −1.89. The energy of this symmetry-broken state lies 32.4 kcal mol^{-1} below the TS1 in Fig. 1. However, computed $\langle S^2 \rangle$ values were far from the correct value (0) expected for a singlet state,[33] due to significant spin contamination from higher spin multiplicities. Such computational analyses are therefore not reliable especially in energetics, and we do not discuss this result anymore. The energetics will be best improved if we use a multiconfigurational method, but such an analysis for dinuclear complexes is difficult to perform at present.

The hydroxy intermediate thus formed is then converted into the product (methanol) complex through a methyl migration via the three-centered transition state (TS2), as indicated in Fig. 1. This transition state has an imaginary mode of vibration (437i cm^{-1}); this low frequency is appropriate for the intramolecular methyl migration. The dissociating Fe–C bond is 2.090 Å and the forming C–O bond is 1.931 Å. The activation barrier for TS2 was computed to be 17.9 kcal mol^{-1}, and we therefore expect that the methyl migration should take place quite easily to make the product complex that includes methanol as a ligand. The features of this methyl migration are also identical to those of the FeO^+/CH_4 case indicated in Scheme 1 in essential bonding characters.[22] Our DFT computations predict that activation energy of about 22.9 kcal mol^{-1} should be required to eliminate the product methanol from the dinuclear complex.

Figure 2 presents a computed energy diagram along the reaction pathway for the conversion of methane to methanol on the diiron model of intermediate **Q** of sMMO. Zero-point energy corrections were taken into account in drawing this energy diagram. At first sight, the potential energy surface is downhill toward the product complex (16.1 kcal mol^{-1} exothermic), and we therefore expect that the direct methane hydroxylation should occur on this dinuclear complex. However, the energy barrier for TS1 is rather high from our computations. Since the two iron active centers of intermediate **Q** have been proposed to be antiferromagnetically coupled,[3] we have confined our discussion above to the reaction species of the singlet state. However, in the context of the "two-state-reactivity" paradigm proposed by Shaik et al.[34] and our computational results[22b] on the C–H cleavage in the FeO^+/CH_4 system, we should consider higher spin states for the C–H cleavage pathway. Spin inversion between different spin multiplicities can in principle reduce the activation barrier for TS1 on the analogy of the FeO^+/CH_4 case. The computed potential energy surface of the triplet state lies approximately 20 kcal mol^{-1} below the singlet surface, but the symmetry-broken singlet surface lies 10 kcal mol^{-1} below the triplet surface. This confusing result clearly comes from the shortcoming of the methods we used—the spin contamination problem inherent in spin-unrestricted calculations. Direct comparison between the singlet and the triplet energies is somewhat difficult to perform within the framework of the one-electron approximation.

Methane–Methanol Conversion on a Dicopper Model. Having described the concerted reaction pathway on the diiron enzyme model, let us next consider the conversion of methane to methanol on the dicopper enzyme model (**2**). From preliminary calculations we found that the quartet potential energy surface lies about 20 kcal mol^{-1} above the doublet potential energy surface. Our discussions can therefore be confined to the reaction pathway on the doublet potential energy surface. Figure 3 presents optimized structures for the reaction intermediates and the transition states that model the reaction pathway for the methane hydroxylation by pMMO. Let us first look at the initial dicopper complex. The computed Cu···Cu distance in the diamond core is 2.915 Å and the O···O distance is 2.399 Å. The Cu···Cu distance is clearly longer than the Fe···Fe distance in model **1**; this result is quite reasonable because high-lying antibonding d-block orbitals of the dicopper model are partly filled while antibonding d-block orbitals of the diiron complex are not filled. The features of these reaction intermediates and transition states are quite similar to those of the diiron model in essential bonding characters. However, there is a remarkable

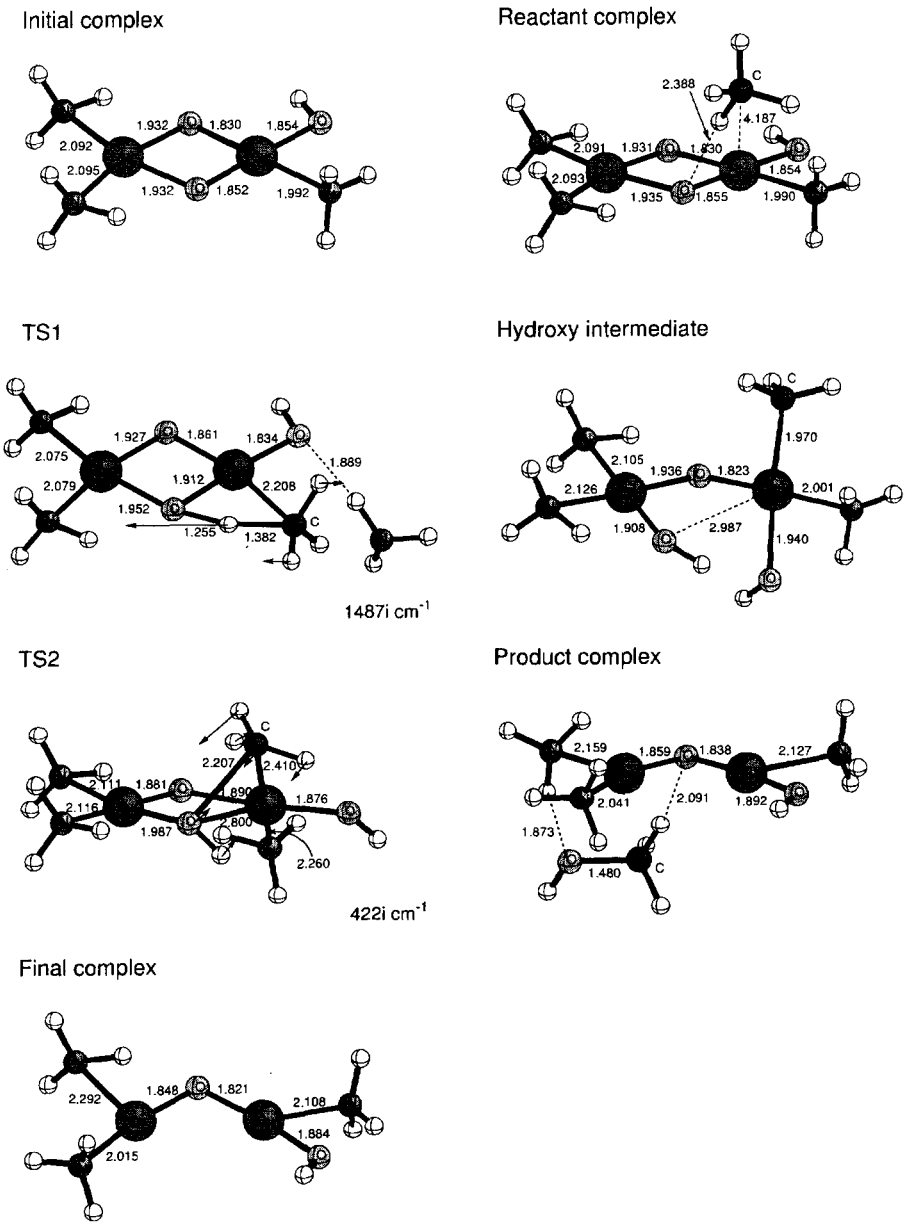

Fig. 3. Computed structures for the reaction intermediates and the transition states (TS1 and TS2) for the conversion of methane to methanol by a dicopper model complex of pMMO (**2**). Bond distances in Å. Imaginary modes of vibration that characterize the transition states are indicated.

contrast between the diiron model and the dicopper model concerning the reactivity toward methane in the initial stages of the reaction.

The binding energy between the methane molecule and the dicopper complex is small (1.2 kcal mol^{-1}) compared to the diiron model complex (6.1 kcal mol^{-1}), but from a vibrational analysis this initial complex was also verified to be a true stable point on the B3LYP potential energy surface. The computed Cu–C(H_4) distance is 4.187 Å, which is much longer than the Fe–C(H_4) distance of 2.831 Å in the case of model **1**; thus, there is little interaction between the methane molecule and the copper ion. Of course, this weak binding is not due to the neutrality of the dicopper complex. The underlying reason is clear from the point of view of orbital interactions. The d-block orbitals of the dicopper model are almost occupied in the Cu(II)-d^9 and Cu(III)-d^8 configuration, while more than half of the d-block orbitals of the diiron model are unoccupied in the Fe(IV)-d^4 configurations. The potential driving force for the binding of methane is orbital interactions, particularly between the t_2 HOMO of methane and unfilled d-block orbitals of the complexes, as discussed previously in terms of second-order perturbation theory.[17b] They are two-orbital two-electron bonding interactions. In particular, nonbonding orbitals coming from a coordinatively unsaturated transition-metal ion of complex play a central role in the binding of the substrate. Therefore the difference in the number of d electrons in the diiron and the dicopper models significantly affects the binding of methane through the orbital interactions, as indicated in Chart 4. The orbital interaction indicated with the wavy line is effec-

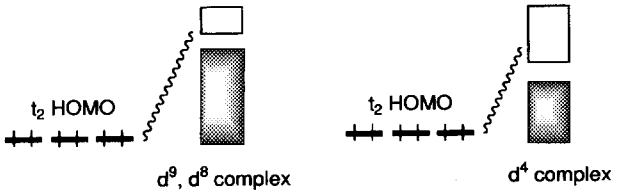

Chart 4.

tively operative in the Fe(IV)-d^4 configuration, but not in the Cu(II)-d^9 and Cu(III)-d^8 configuration. The two-orbital four-electron interactions between the filled orbitals of the substrate and the complex are repulsive and are one primary source of barriers to the formation of methane complex. This is a good reason for the computational results that methane is tightly bound to the diiron model but is not effectively bound to the dicopper model.

Although methane is not effectively bound to the dicopper complexes from B3LYP computations, H atom abstraction of methane takes place in a similar way via the four-centered transition state TS1, as presented for model **2** in Fig. 3. TS1 in model **2** is characterized by a single imaginary mode of vibration (1487i cm^{-1}) which is responsible for the C–H bond dissociation and the O–H bond formation. The four-centered transition state is quite similar to that of the diiron model (**1**). The dissociating C–H bond of 1.382 Å and the forming O–H bond of 1.255 Å are again appropriate for this concerted electronic process. Since a copper ion prefers a square-planar structure, one of the ammonia ligands is replaced by the coordinating methane molecule. The activation barrier for TS1 was computed to be 40.5 kcal mol^{-1} on the doublet potential energy surface. The resultant hydroxy intermediate, which involves four-coordinate copper ions, is then converted into the product (methanol) complex through a methyl migration via the three-centered transition state (TS2), which has an imaginary mode of 422i cm^{-1}. The optimized structure for this transition state is in good agreement with that in the diiron model in essential bonding characters. In contrast to the diiron complex case, the product methanol is not bound to the copper ions of the model complex. This is again due to the different numbers of d electrons in the diiron and the dicopper models.

Figure 4 shows a computed energy diagram of the spin-doublet reaction pathway for the conversion of methane to methanol on the dicopper model of pMMO. The total reaction is 7.3 kcal mol^{-1} exothermic. We found from preliminary DFT computations that the quartet potential energy surface lies about 20 kcal mol^{-1} above the doublet surface, as indicated earlier in this paper. There is no crossing of potential energy surfaces of the different spin states, and we therefore expect that this reaction should occur preferentially on the doublet potential energy surface. The essential features of the two methane-methanol conversion pathways presented in Figs. 2 and 4 are identical, especially in the geometrical structures of the first and the second transition states.

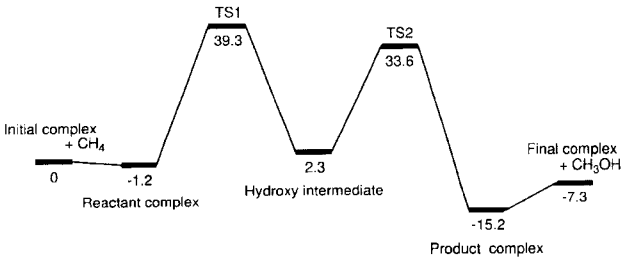

Fig. 4. Energetics for the conversion of methane to methanol by a dicopper model complex of pMMO (**2**). Energies in kcal mol^{-1}.

We have computed a methane–methanol conversion pathway using a different dicopper model (**3**) that involves three- and four-coordinate copper ions, but the computational results were essentially identical to those for model **2**. Thus, we do not repeat the results anymore. The reader can see in Figs. 5 and 6 optimized structures of the reaction species and the energetics along the reaction pathway.

Direct H Atom Abstraction on Diiron and Dicopper Models. There is a widely-believed radical mechanism for H atom abstraction of substrate hydrocarbons, which is called "oxygen rebound mechanism".[15] Until now in this article we have not referred to the radical mechanism for the direct H atom abstraction by the oxo species of cytochrome P450 in order to concentrate on our two-step concerted mechanism. The oxygen rebound mechanism is in remarkable contrast to our concerted mechanism via the four-centered transition state (TS1) discussed above in that the iron ion plays no significant role in this radical process while it is a major contributor in the concerted process. Siegbahn and Crabtree[16] have proposed from DFT-computational analyses using realistic diiron models that the direct H atom abstraction should take place in the initial stages of the methane hydroxylation by sMMO. Recently Basch et al.[35] also proposed a similar radical mechanism. Vibrational analyses were not carried out in their DFT calculations, due to large diiron models. In contrast to their proposals, the regioselectivity observed in the P450- and sMMO-catalyzed hydroxylation of methylcubane considerably differs from that found in the *t*-BuO· radical abstraction.[20] In particular, sMMO hydroxylase from *Methylococcus capsulatus* (Bath) yields products corresponding only to oxidation at the methyl position of the substrate. The experimental results on the marked preference for the primary-carbon position cannot be rationally explained by a simple radical mechanism. Thus, the lack of reactivity at the cubyl C–H bonds would argue against the widely-accepted oxygen rebound mechanism in the enzymatic hydroxylation. One of the authors compared these important experiments and our theoretical predictions in a review paper.[36]

We also found the transition states for the direct H atom abstraction (TSd) in the undecet (S = 5) spin state of the diiron model of sMMO (**1**) and in the doublet state of the dicopper model of pMMO (**2**). Ball-and-stick structures for these transition states are shown in Fig. 7. In the diiron model the C–H and O–H distances were optimized as 1.228 and 1.328 Å, respectively, and in the dicopper model the C–H and the O–H distances were computed to be 1.455 and 1.113 Å, respectively. These C–H and O–H distances are likely

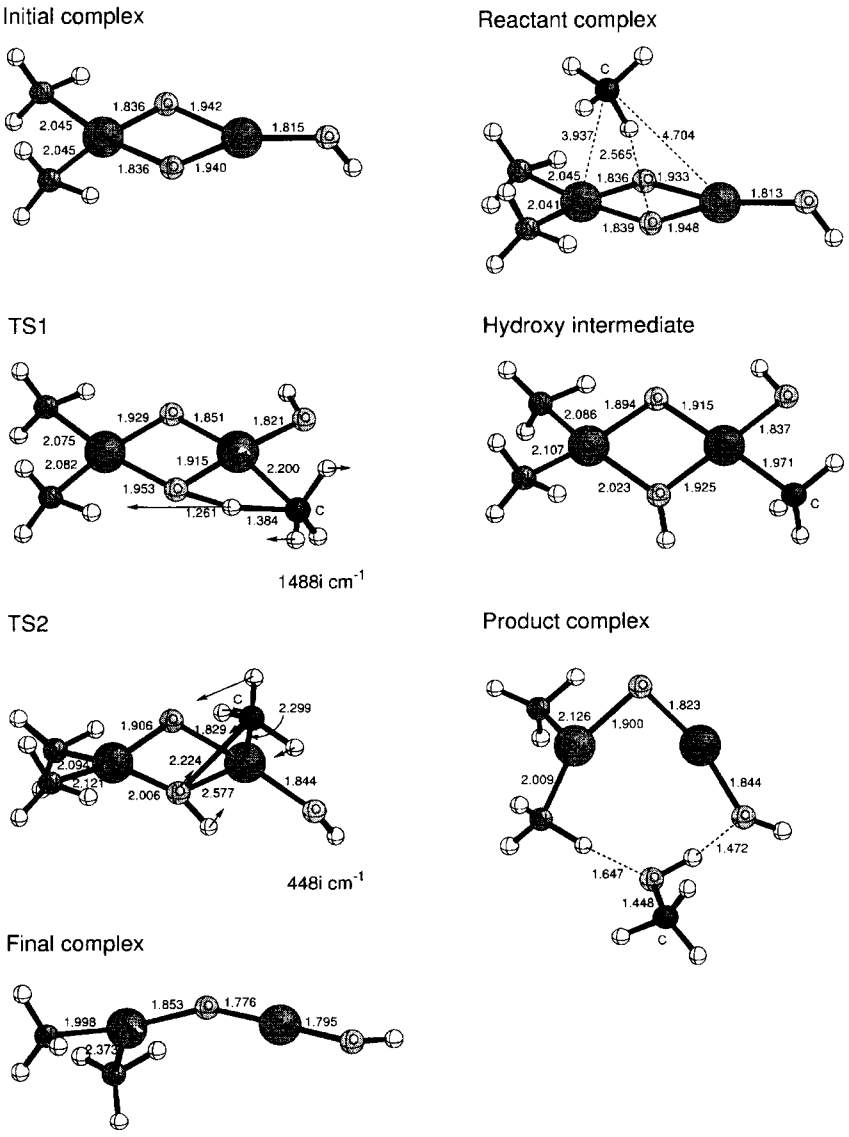

Fig. 5. Computed structures for the reaction intermediates and the transition states (TS1 and TS2) for the conversion of methane to methanol by a dicopper model complex of pMMO (**3**). Bond distances in Å. Imaginary modes of vibration that characterize the transition states are indicated.

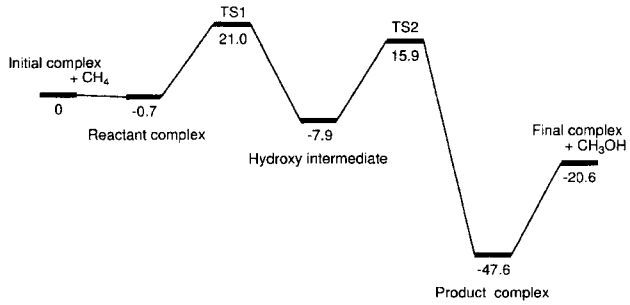

Fig. 6. Energetics for the conversion of methane to methanol by a dicopper model complex of pMMO (**3**). Energies in kcal mol^{-1}.

to be appropriate for these direct abstraction processes. The transition metals do not play a central role in the direct processes, in remarkable contrast to our concerted mechanism discussed earlier. Thus, the direct H atom abstraction is a simple electronic process for the C–H bond dissociation and the O–H bond formation; the radical character of the oxo species can determine whether the direct process occurs or not. However, because of inherent spin-contamination in the spin-unrestricted method, we cannot decide which of the proposed mechanisms is more favorable in energy.

As indicated in our previous paper,[22c] the direct H atom abstraction of methane occurs in the high-spin sextet state of the bare FeO^+ complex, but not in the low-spin quartet state, which is in good agreement with the present results on the dinuclear iron model. In spite of our best efforts, such a transition state was not found in the low-spin quartet state of the FeO^+/CH_4 system. This computational result may be reasonable in view of the frontier orbitals of FeO^+ in Chart 5 because the 3σ orbital of FeO^+, the amplitude of which exists on the oxygen atom in some degree, is singly occupied in the high-spin sextet state and accordingly the radical character of the oxygen atom, which can play a major

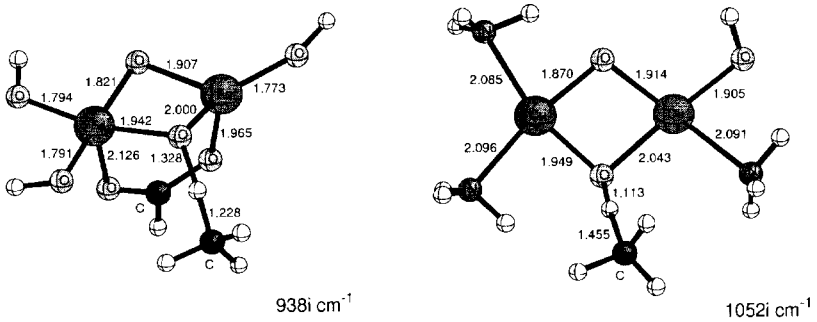

Fig. 7. Computed structures for the transition states for the direct H atom abstraction on a diiron complex (**1**) of the undecet state and a dicopper model complex (**2**) of the doublet state.

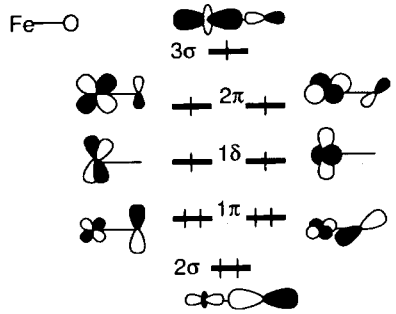

Chart 5.

role in the direct H atom abstraction, is significant in the sextet state. However, this 3σ orbital is vacant in the low-spin quartet state, and therefore the spin density on the oxygen atom is significantly diminished in the quartet state. In fact, computed spin densities of the oxygen atom are 1.14 and −0.63 in the sextet and the quartet states, respectively. As a result, the direct H atom abstraction occurs in the high-spin sextet state, but the transition state for the direct abstraction lie 4 kcal mol^{-1} above TS1 of the quartet state.[22c]

Figure 8 shows the d-block orbitals of model **1**. MOLDEN[37] was used for molecular orbital visualizations. We can consider from these d-block orbitals why the direct H atom abstraction occurs in the undecet state of the diiron complex. In the singlet state the 49th orbital is the HOMO, and in the undecet state the 54th orbital is the highest SOMO (singly occupied molecular orbital). Note that the 54th and 55th orbitals are of σ type with respect to an Fe–O bond, and they are similar to the 3σ orbital of the bare FeO^+ complex in Chart 5. Therefore, if these σ-type orbitals are singly occupied, the radical character of the oxo species increases; we expect that the direct H atom abstraction should occur in the undecet state on the analogy of the FeO^+/CH_4 case. Thus, our computational result that the direct H atom abstraction occurs in the undecet state can be rationalized in view of the frontier orbitals of the diiron model.

Let us next look at the d-block orbitals of model **2** indicated in Fig. 9. The orbitals are simple compared to those of **1**, due to the pseudo-D_{2h} symmetry of the diamond core of **2**. Since the number of d electrons is larger in copper, the d-block orbitals of the dicopper model are doubly occupied, except for the highest two orbitals. The 47th and 48th orbitals of **2** are very similar to the 54th and 55th orbitals of **1** in that these d-block orbitals are of σ type with respect to the metal–oxygen bonds in the diamond cores. Since in the doublet state of **2**, the 47th orbital is the highest SOMO, the direct H atom abstraction is expected to occur in the doublet state of model **2**. We therefore think that the direct H atom abstraction should be preferred in the dicopper complex rather than in the diiron complex. The aliphatic ligand hydroxylation observed on a dicopper complex[13] has been proposed to result from such direct H atom abstraction of ligand. In any case, the σ-type orbitals of the dinuclear complexes play an essential role in the direct H atom abstraction of hydrocarbon substrates.

The distance between the transition-metal ions and the migrating H atom in TS1 is about 1.7—1.8 Å,[22b] so there are direct interactions between them. Moreover, there is a metal–carbon bond in TS1, as indicated in Figs. 1 and 3. We believe that such bonding interactions would energetically stabilize the four-centered transition state (TS1) to facilitate the cleavage of the strong C–H bond of methane, the most inert hydrocarbon. The formation of such a metal–carbon bond may have relevance to the mechanism of *Gif* chemistry proposed by Barton and collaborators.[38] If a catalytically active metal center is coordinatively unsaturated, such a four-centered transition-state structure is likely to be quite reasonable. We recently confirmed from detailed IRC (intrinsic

Table 2. Computed Values of the Kinetic Isotope Effect (k_H/k_D) for the C–H(D) Dissociation of Methane on Diiron Model **1**, and Dicopper Model **2**
TS1 and TSd stand for the four-centered concerted transition state and the direct-abstraction transition state, respectively. The numbers in the parentheses are spin multiplicities (2*S*+1).

T (K)	**1** TS1 (1)	**1** TS1 (3)	**1** TSd (11)	**2** TS1 (2)	**2** TSd (2)
250	11.14	12.07	14.95	12.86	24.95
260	10.55	11.38	13.87	12.08	22.79
270	9.99	10.76	12.86	11.39	20.78
280	9.47	10.18	12.02	10.78	19.10
290	9.03	9.68	11.27	10.23	17.64
300	8.60	9.21	10.58	9.71	16.34
310	8.24	8.80	9.99	9.25	15.20
320	7.88	8.39	9.45	8.83	14.18
330	7.56	8.05	8.96	8.44	13.28
340	7.26	7.72	8.52	8.09	12.47
350	6.99	7.41	8.12	7.76	11.76

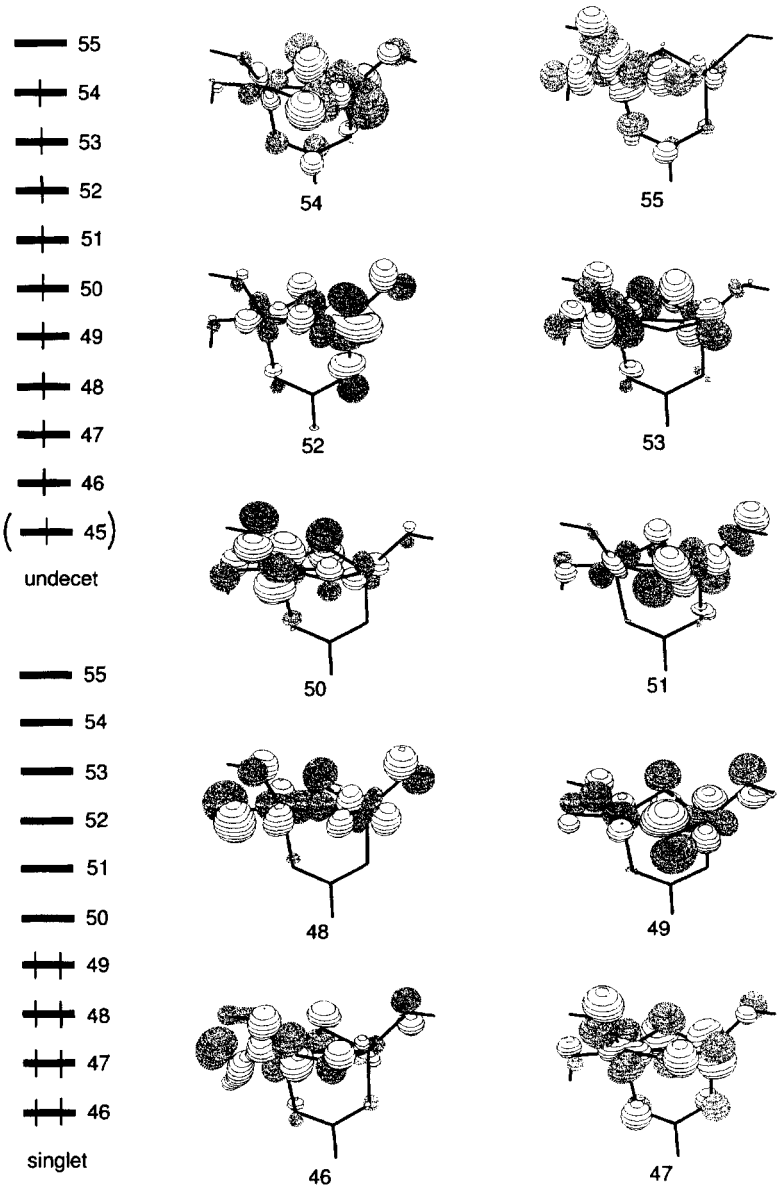

Fig. 8. The d-block orbitals of a diiron model complex (**1**).

reaction coordinate) analyses[39] that TS1 and TS2 correctly connect the concerted reaction pathway for the gas-phase methane hydroxylation by the FeO^+ complex.[40]

Kinetic Isotope Effects. Having described the different C–H dissociation mechanisms, we next address the kinetic isotope effects (k_H/k_D), which can be calculated from vibrational analyses with the transition-state theory.[41] The k_H/k_D value is an important measure in discussing how H atom abstraction of a hydrocarbon substrate takes place in catalytic and enzymatic systems. The values of k_H/k_D were obtained from the following equation:[42]

$$\frac{k_{CH_4}}{k_{CD_4}} = \left(\frac{m^R_{CD_4} m^\#_{CH_4}}{m^R_{CH_4} m^\#_{CD_4}}\right)^{3/2} \left(\frac{I_{CD_4}}{I_{CH_4}}\right)^{3/2} \left(\frac{I^\#_{xCH_4} I^\#_{yCH_4} I^\#_{zCH_4}}{I^\#_{xCD_4} I^\#_{yCD_4} I^\#_{zCD_4}}\right)^{1/2} \times \frac{q^R_{\nu CD_4} q^\#_{\nu CH_4}}{q^R_{\nu CH_4} q^\#_{\nu CD_4}} \exp\left(-\frac{E^\#_{CH_4} - E^\#_{CD_4}}{RT}\right), \quad (1)$$

where superscripts R and # specify the reactant methane and the transition state, respectively, for the molecular mass m, the moment of inertia I, the vibrational partition function q, and the activation energy E. The last exponential term is dominant in this equation because the other terms can be almost all canceled between denominators and numerators. The numerator in the last exponential term comes from the fact that C–H dissociation has a lower activation energy than C–D dissociation on account of the former's greater zero-point vibrational energy.

Table 2 summarizes calculated values of k_H/k_D for the concerted abstraction via TS1 of the diiron model and the dicopper models and for the direct abstraction via TSd as a function of temperature. At 300 K, the concerted transition states (TS1) gave k_H/k_D values of 8.60—9.71 while the direct abstraction transition states (TSd) gave k_H/k_D values of 10.58—16.34. As expected and calculated, the direct abstraction transition states afford larger values of k_H/k_D than the concerted transition state. These theoretical analyses are

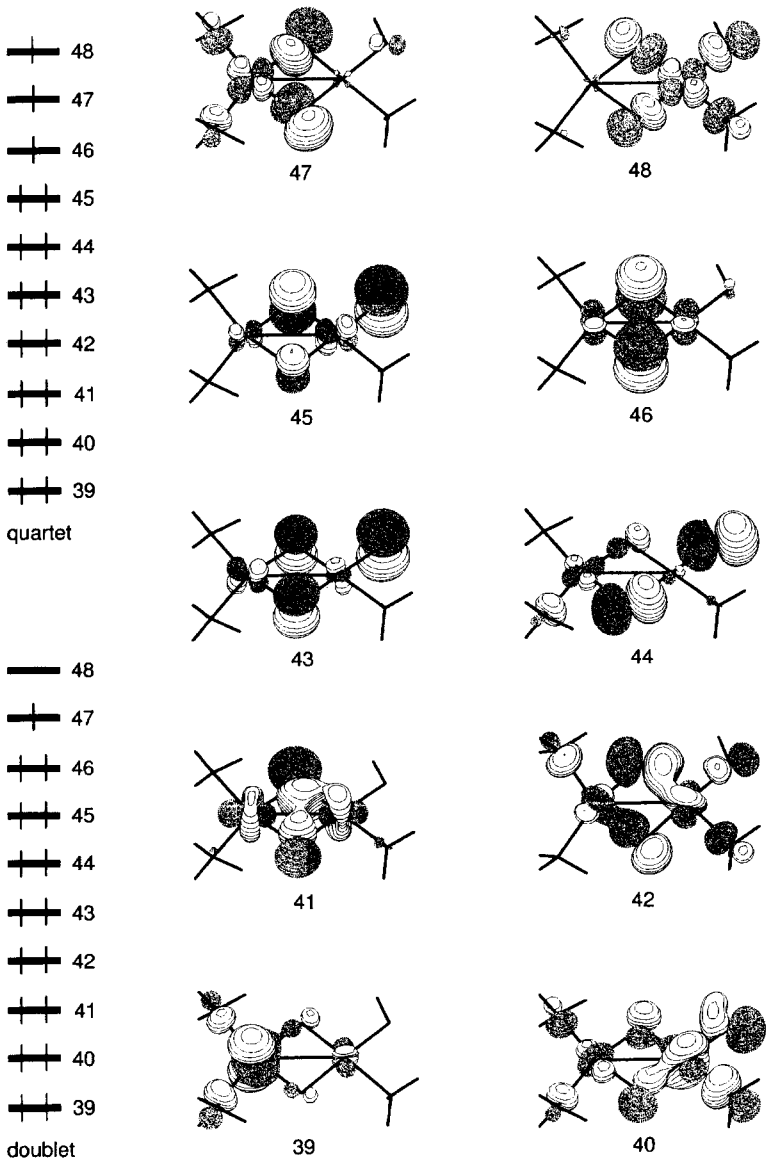

Fig. 9. The d-block orbitals of a dicopper model complex (**2**).

very important in discussing the mechanism of P450- and MMO-catalyzed hydrocarbon hydroxylation.

Conclusions

We have described theoretical analyses for the conversion of methane to methanol on a diiron model of soluble methane monooxygenase (sMMO) and on dicopper models of particulate methane monooxygenase (pMMO). A strong point in this study is in the systematic vibrational analyses, which enabled us to perform detailed characterizations of potential energy surfaces and kinetic isotope effects for the H(D) atom abstractions of methane. Methane is reasonably converted to methanol on the diiron and dicopper enzyme models in a two-step concerted manner. The first step in our proposal is concerted H atom abstraction of methane via a four-centered transition state (TS1) and the second step is concerted methyl migration via a three-centered transition state (TS2). The general features of this electronic process are identical to those of the gas-phase process for the methane–methanol conversion by the bare FeO^+ complex. The transition state for the direct H atom abstraction (TSd) on the diiron model was found in a very high-spin state, and that on the dicopper models are found in a doublet state. The reasons why we prefer the four-centered transition state are that the transition-metal ions significantly contribute to the transition state, in contrast to the direct abstraction in which the transition-metal ions are a spectator, and that this concerted mechanism is consistent with the sMMO-catalyzed regioselective hydroxylation of methylcubane. We need further detailed analyses to conclude which of the mechanisms is energetically more favorable. We finally calculated and analyzed kinetic isotope effects for the concerted and the direct H atom abstraction mechanisms using the transition state theory. Computed values of k_H/k_D for TS1 and TSd are 9 and 14 on average, respectively, at 300 K.

K. Y. is grateful for a Grant-in-Aid for Scientific Research on the Priority Area "Molecular Biometallics" from the Min-

istry of Education, Science, Sports and Culture in support of this work. Y. S. is grateful to the JSPS for a graduate fellowship. Computations were in part carried out in the Supercomputer Laboratory of Kyoto University and in the Computer Center of the Institute for Molecular Science.

Appendix

As suggested by a reviewer of this paper, it is difficult to conclude from our computations that the concerted mechanism is energetically preferable to the radical mechanism for the enzymatic reaction. We must admit this comment at present. However, we believe that our concerted mechanism is right mainly from the three points: (1) no radical mechanism can explain the regioselective experiments in the hydroxylation of methylcubane by sMMO,[20] as discussed in the text, (2) the observed active site of intermediate **Q** is coordinatively unsaturated,[5] and (3) from known catalytic chemistry or organometallic chemistry, it is quite reasonable to assume that catalytically active centers should be coordinatively unsaturated for substrate binding. Our mechanism can explain observed KIEs, inversion of stereochemistry, and timescales measured from radical clocks, as discussed previously in our papers.[24,36,43]

References

1 Recent reviews on sMMO: a) B. J. Wallar and J. D. Lipscomb, *Chem. Rev.*, **96**, 2625 (1996). b) L. Que, Jr., and Y. Dong, *Acc. Chem. Res.*, **29**, 190 (1996). c) D. M. Kurtz, Jr., *J. Biol. Inorg. Chem.*, **2**, 159 (1997). d) K. K. Andersson and A. Gräslund, *Adv. Inorg. Chem.*, **43**, 359 (1995). e) A. L. Feig and S. J. Lippard, *Chem. Rev.*, **94**, 759 (1994). f) J. D. Lipscomb, *Annu. Rev. Microbiol.*, **48**, 371 (1994). g) S. J. Lippard, *Angew. Chem., Int. Ed. Engl.*, **27**, 344 (1988).

2 X-Ray structural analyses for some forms of sMMO: a) A. C. Rosenzweig, C. A. Frederick, S. J. Lippard, and P. Nordlund, *Nature*, **366**, 537 (1993). b) A. C. Rosenzweig and S. J. Lippard, *Acc. Chem. Res.*, **27**, 229 (1994). c) A. C. Rosenzweig, P. Nordlund, P. M. Takahara, C. A. Frederick, and S. J. Lippard, *Chem. Biol.*, **2**, 409 (1995). d) A. C. Rosenzweig, H. Brandstetter, D. A. Whittington, P. Nordlund, S. J. Lippard, and C. A. Frederick, *Proteins: Struct. Func. Genetics*, **29**, 141 (1997).

3 S. K. Lee, B. G. Fox, W. A. Froland, J. D. Lipscomb, and E. Münck, *J. Am. Chem. Soc.*, **115**, 6450 (1993).

4 a) K. E. Liu, A. M. Valentine, D. Wang, B. H. Huynh, D. E. Edmondson, A. Salifoglou, and S. J. Lippard, *J. Am. Chem. Soc.*, **117**, 10174 (1995). b) A. M. Valentine, S. S. Stahl, and S. J. Lippard, *J. Am. Chem. Soc.*, **121**, 3876 (1999).

5 L. Shu, J. C. Nesheim, K. Kauffmann, E. Münck, J. D. Lipscomb, and L. Que, Jr., *Science*, **275**, 515 (1997).

6 a) R. J. Deeth and H. Dalton, *J. Biol. Inorg. Chem.*, **3**, 302 (1998). b) D. A. Whittington, A. M. Valentine, and S. J. Lippard, *J. Biol. Inorg. Chem.*, **3**, 307 (1998). c) P. E. M. Siegbahn, R. H. Crabtree, and P. Nordlund, *J. Biol. Inorg. Chem.*, **3**, 314 (1998). d) K. Yoshizawa, *J. Biol. Inorg. Chem.*, **3**, 318 (1998). e) A. A. Shteinman, *J. Biol. Inorg. Chem.*, **3**, 325 (1998). f) J. D. Lipscomb and L. Que, Jr., *J. Biol. Inorg. Chem.*, **3**, 331 (1998).

7 a) H.-H. T. Nguyen, A. K. Shiemke, S. J. Jacobs, B. J. Hales, M. E. Lidstrom, and S. I. Chan, *J. Biol. Chem.*, **269**, 14995 (1994). b) J. D. Semrau, D. Zolandz, M. E. Lidstrom, and S. I. Chan, *J. Inorg. Biochem.*, **58**, 235 (1995).

8 H. Yuan, M. L. P. Collins, and W. E. Antholine, *J. Am. Chem. Soc.*, **119**, 5073 (1997).

9 M. Takeguchi, K. Miyakawa, and I. Okura, *J. Mol. Catal. A*, **132**, 145 (1998).

10 a) B. Wilkinson, M. Zhu, N. D. Priestley, H.-H. T. Nguyen, H. Morimoto, P. G. Williams, S. I. Chan, and H. G. Floss, *J. Am. Chem. Soc.*, **118**, 921(1996). b) S. J. Elliott, M. Zhu, L. Tso, H.-H. T. Nguyen, J. H.-K. Yip, and S. I. Chan, *J. Am. Chem. Soc.*, **119**, 9949 (1997).

11 a) E. Pidcock, H. V. Obias, X. Zhang, K. D. Karlin, and E. I. Solomon, *J. Am. Chem. Soc.*, **120**, 7841 (1998). b) H. V. Obias, Y. Lin, N. N. Murthy, E. Pidcock, E. I. Solomon, M. Ralle, N. J. Blackburn, Y.-M. Neuhold, A. D. Zuberbühler, and K. D. Karlin, *J. Am. Chem. Soc.*, **120**, 12960 (1998).

12 a) J. A. Halfen, S. Mahapatra, E. C. Wilkinson, S. Kaderli, V. G. Young, Jr., L. Que, Jr., A. D. Zuberbüler, and W. B. Tolman, *Science*, **271**, 1397(1996). b) S. Mahapatra, J. A. Halfen, E. C. Wilkinson, G. Pan, X. Wang, V. G. Young, Jr., C. J. Cramer, L. Que, Jr., and W. B. Tolman, *J. Am. Chem. Soc.*, **118**, 11555 (1996). c) S. Mahapatra, V. G. Young, Jr., S. Kaderli, A. D. Zuberbüler, and W. B. Tolman, *Angew. Chem., Int. Ed. Engl.*, **36**, 130 (1997).

13 S. Itoh, H. Nakao, L. M. Berreau, T. Kondo, M. Komatsu, and S. Fukuzumi, *J. Am. Chem. Soc.*, **120**, 2890 (1998).

14 a) S. Hikichi, H. Komatsuzaki, M. Akita, and Y. Moro-oka, *J. Am. Chem. Soc.*, **120**, 4699 (1998). b) S. Hikichi, M. Yoshizawa, Y. Sasakura, M. Akita, and Y. Moro-oka, *J. Am. Chem. Soc.*, **120**, 10567 (1998).

15 P. R. Ortiz de Montellano, "Cytochrome P450: Structure, Mechanism, and Biochemistry," 2nd ed, Plenum, New York (1995).

16 a) P. E. M. Siegbahn and R. H. Crabtree, *J. Am. Chem. Soc.*, **119**, 3103 (1997). b) P. E. M. Siegbahn, *Inorg. Chem.*, **38**, 2880 (1999).

17 a) K. Yoshizawa and R. Hoffmann, *Inorg. Chem.*, **35**, 2409 (1996). b) K. Yoshizawa, T. Yamabe, and R. Hoffmann, *New J. Chem.*, **21**, 151 (1997). c) K. Yoshizawa, T. Ohta, T. Yamabe, and R. Hoffmann, *J. Am. Chem. Soc.*, **119**, 12311 (1997). d) K. Yoshizawa, T. Ohta, and T. Yamabe, *Bull. Chem. Soc. Jpn.*, **71**, 1899 (1998).

18 a) B. G. Fox, W. A. Froland, J. Dege, and J. D. Lipscomb, *J. Biol. Chem.*, **264**, 10023 (1989). b) J. Green and H. Daltom, *J. Biol. Chem.*, **264**, 17698 (1989). c) B. G. Fox, J. G. Borneman, L. P. Wackett, and J. D. Lipscomb, *Biochemistry*, **29**, 6419 (1990). d) N. Deighton, I. D. Podmore, M. C. R. Symons, P. C. Wilkins, and H. Dalton, *J. Chem. Soc., Chem. Commun.*, **1991**, 1086. e) N. D. Priestley, H. G. Floss, W. A. Froland, J. D. Lipscomb, P. G. Williams, and H. Morimoto, *J. Am. Chem. Soc.*, **114**, 7561 (1992).

19 K. E. Liu, C. C. Johnson, M. Newconb, and S. J. Lippard, *J. Am. Chem. Soc.*, **115**, 939 (1993).

20 S.-Y. Choi, P. E. Eaton, P. F. Hollenberg, K. E. Liu, S. J. Lippard, M. Newcomb, D. A. Putt, S. P. Upadhyaya, and Y. Xiong, *J. Am. Chem. Soc.*, **118**, 6547 (1996).

21 A. M. Valentine, B. Wilkinson, K. E. Liu, S. Komar-Panicucci, N. D. Priestley, P. G. Williams, H. Morimoto, H. G. Floss, and S. J. Lippard, *J. Am. Chem. Soc.*, **119**, 1818 (1997).

22 a) K. Yoshizawa, Y. Shiota, and T. Yamabe, *Chem. Eur. J.*, **3**, 1160 (1997). b) K. Yoshizawa, Y. Shiota, and T. Yamabe, *J. Am. Chem. Soc.*, **120**, 564 (1998). c) K. Yoshizawa, Y. Shiota, and T. Yamabe, *Organometallics*, **17**, 2825 (1998).

23 a) D. Schröder and H. Schwarz, *Angew. Chem., Int. Ed. Engl.*, **29**, 1433 (1990). b) D. Schröder, A. Fiedler, J. Hrusák, and H. Schwarz, *J. Am. Chem. Soc.*, **114**, 1215 (1992). c) D. Schröder, H. Schwarz, D. E. Clemmer, Y. -M. Chen, P. B. Armentrout, V. I. Baranov, and D. K. Böhme, *Int. J. Mass Spectrum. Ion Processes*,

161, 175 (1997).

24 K. Yoshizawa, Y. Shiota, Y. Kagawa, and T. Yamabe, *J. Phys. Chem. A*, in press.

25 K. Yoshizawa, Y. Shiota, and T. Yamabe, *J. Am. Chem. Soc.*, **121**, 147 (1999).

26 M. J. Frisch, G. W. Trucks, H. B. Schlegel, G. E. Scuseria, M. A. Robb, J. R. Cheeseman, V. G. Zakrzewski, J. A. Montgomery, R. E. Stratmann, J. C. Burant, S. Dapprich, J. M. Millam, A. D. Daniels, K. N. Kudin, M. C. Strain, O. Farkas, J. Tomasi, V. Barone, M. Cossi, R. Cammi, B. Mennucci, C. Pomelli, C. Adamo, S. Clifford, J. Ochterski, G. A. Petersson, P. Y. Ayala, Q. Cui, K. Morokuma, D. K. Malick, A. D. Rabuck, K. Raghavachari, J. B. Foresman, J. Cioslowski, J. V. Ortiz, B. B. Stefanov, G. Liu, A. Liashenko, P. Piskorz, I. Komaromi, R. Gomperts, R. L. Martin, D. J. Fox, T. Keith, M. A. Al-Laham, C. Y. Peng, A. Nanayakkara, C. Gonzalez, M. Challacombe, P. M. W. Gill, B. G. Johnson, W. Chen, M. W. Wong, J. L. Andres, M. Head-Gordon, E. S. Replogle, and J. A. Pople, "Gaussian 98," Gaussian Inc., Pittsburgh, PA (1998).

27 a) A. D. Becke, *Phys. Rev. A*, **A38**, 3098 (1988). b) A. D. Becke, *J. Chem. Phys.*, **98**, 5648 (1993).

28 C. Lee, W. Yang, and R. G. Parr, *Phys. Rev. B*, **B37**, 785 (1988).

29 P. J. Hay and W. R. Wadt, *J. Chem. Phys.*, **82**, 299 (1985).

30 T. H. Dunning, Jr., and P. J. Hay, "Modern Theoretical Chemistry," ed by H. F. Schaefer, III, Plenum, New York (1976), p. 1.

31 a) N. Koga and K. Morokuma, *J. Phys. Chem.*, **94**, 5454 (1990). b) N. Koga and K. Morokuma, *J. Am. Chem. Soc.*, **115**, 6883 (1993). c) D. G. Musaev, N. Koga, and K. Morokuma, *J. Phys. Chem.*, **97**, 4064 (1993). d) D. G. Musaev and K. Morokuma, *J. Phys. Chem.*, **100**, 11600 (1996).

32 a) D. J. Trevor, D. M. Cox, and A. Kaldor, *J. Am. Chem. Soc.*, **112**, 3742 (1990). b) K. K. Irikura and J. L. Beauchamp, *J. Phys. Chem.*, **95**, 8344 (1991). c) Y. A. Ranasinghe, T. J. MacMahon, and B. S. Freiser, *J. Phys. Chem.*, **95**, 7721 (1991). d) R. J. Van Zee, S. Li, and W. Weltner, Jr., *J. Am. Chem. Soc.*, **115**, 2976 (1993). e) J. J. Carrol and J. C. Weisshaar, *J. Am. Chem. Soc.*, **115**, 800 (1993). f) P. Burger and R. G. Bergman, *J. Am. Chem. Soc.*, **115**, 10462 (1993). g) C. P. Schaller, J. B. Bonanno, and P. T. Wolczanski, *J. Am. Chem. Soc.*, **116**, 4133 (1994). h) X. -X. Zhang and B. B. Wayland, *J. Am. Chem. Soc.*, **116**, 7897 (1994). i) W. E. Billups, S. -C. Chang, R. H. Hauge, and J. L. Margrave, *J. Am. Chem. Soc.*, **117**, 1387 (1995). j) P. A. M. van Koppen, P. R. Kemper, J. E. Bushnell, and M. T. Bowers, *J. Am. Chem. Soc.*, **117**, 2098 (1995). k) M. L. Campbell, *J. Am. Chem. Soc.*, **119**, 5984 (1997).

33 Computed $\langle S^2 \rangle$ value for the TS1 of the symmetry-broken singlet state are 2.28 and 6.57 before and "after" annihilation of higher spin multiplicities, respectively, thus the wavefunction being not a pure singlet, but a mixture of singlet, triplet, quintet, and septet spin states.

34 a) S. Shaik, D. Danovich, A. Fiedler, D. Schröder, and H. Schwarz, *Helv. Chim. Acta*, **78**, 1393 (1995). b) S. Shaik, M. Filatov, D. Schröder, and H. Schwarz, *Chem. Eur. J.*, **4**, 193 (1998).

35 H. Basch, K. Mogi, D. G. Musaev, and K. Morokuma, *J. Am. Chem. Soc.*, **121**, 7249 (1999).

36 K. Yoshizawa, *J. Inorg. Biochem.*, **78**, 23 (2000).

37 G. Schaftenaar, "MOLDEN," CAOS/CAMM Center Nijmegen, The Netherlands (1991).

38 a) D. H. R. Barton and D. Doller, *Acc. Chem. Res.*, **25**, 504 (1992). b) D. H. R. Barton, and B. Hu, *Pure Appl. Chem.*, **69**, 1941 (1997).

39 K. Fukui, *J. Phys. Chem.*, **74**, 4161 (1970).

40 K. Yoshizawa, Y. Shiota, and T. Yamabe, *J. Chem. Phys.*, **111**, 538 (1999).

41 D. A. McQuarrie, "Statistical Thermodynamics," University Science Books, Mill Valley (1973).

42 M. Filatov and S. Shaik, *J. Phys. Chem. A*, **102**, 3835 (1998).

43 K. Yoshizawa, A. Suzuki, and T. Yamabe, *J. Am. Chem. Soc.*, **121**, 5266 (1999).